

## New information on parton distributions

A. D. Martin and W. J. Stirling

*Department of Physics, University of Durham, Durham DH1 3LE, England*

R. G. Roberts

*Rutherford Appleton Laboratory, Chilton, Didcot OX11 0QX, England*

(Received 5 May 1992; revised manuscript received 28 August 1992)

New data on structure functions from deep-inelastic scattering provide new information on parton distributions, particularly in the  $0.01 < x < 0.1$  interval. This has important implications for predictions for the DESY  $ep$  collider HERA and for present and future high-energy hadron colliders. We present the results of updated fits to all available precision structure function and related data. We focus in particular on two issues: (a) the increase in the sea-quark distributions at small  $x$  implied by new  $F_2$  data from the New Muon Collaboration, and its implications for other processes, and (b) the evidence for SU(2)-symmetry breaking in the light-quark sea. We show that although good fits can be obtained with or without this symmetry breaking, more physically reasonable parton distributions are obtained if we allow  $\bar{d} > \bar{u}$  at small  $x$ . With the inclusion of the latest deep-inelastic data we find  $\alpha_s(M_Z) = 0.111^{+0.004}_{-0.005}$ . We also show how  $W$ ,  $Z$ , and Drell-Yan production at  $\bar{p}p$  colliders can give information on parton distributions.

PACS number(s): 13.60.Hh; 12.38.Bx; 13.15.Dk

### I. INTRODUCTION

Recent determinations [1] of parton distributions have been based on analyses of precision deep-inelastic data which extend down to  $x \sim 0.07$  for  $Q^2 \gtrsim 5 \text{ GeV}^2$ . One or two measurements do exist at lower values of  $x$ , but a full range of precision data for both muon and neutrino deep-inelastic scattering on nucleons has only been available for  $x \gtrsim 0.07$ . As a consequence there is an increasingly wide spread in the behavior of the different sets of parton distributions as they are extrapolated to smaller  $x$  values [2].

The behavior of the parton distributions in the small- $x$  region,  $x \lesssim 0.1$ , is of considerable importance both theoretically and phenomenologically. First, the predictions of the rates of various processes which occur at the high-energy hadron colliders depend on the parton densities at small  $x$ . The distributions at small  $x$  are also needed for comparison with the measurements soon to be made at the DESY  $ep$  collider HERA. From a theoretical point of view the behavior in the very small- $x$  region is particularly interesting since new effects are expected to emerge [3]. Indeed, one of the most important predictions of perturbative QCD is the strong increase of the gluon and sea-quark distributions in the  $x \rightarrow 0$  limit.

There are two main reasons why it is now timely to carry out a new (next-to-leading-order) global structure function analysis and why it should yield much improved parton distributions. First, two new sets of accurate deep-inelastic data, which extend the precision measurements to smaller  $x$  values, have just become available. These are measurements of deep-inelastic scattering of muons on protons and on deuterons by the New Muon Collaboration (NMC) [4], and of neutrinos on iron nuclei by the Chicago-Columbia-Fermilab-Rochester

(CCFR) Collaboration [5]. These latter data differ significantly from the earlier CERN-Dortmund-Heidelberg-Saclay-Warsaw (CDHSW) Collaboration neutrino data [6]; interestingly the  $Q^2$  behavior predicted by the partons resulting from our previous analysis [7], which incorporated the CDHSW neutrino data, is in better agreement with the new CCFR data than with the fitted CDHSW data.

All previous global structure function analyses have assumed that  $\bar{u}(x, Q^2) = \bar{d}(x, Q^2)$ , that is that the light-quark sea distributions are flavor independent. However, based on their  $F_2^n/F_2^p$  measurements, NMC found that [8]

$$\begin{aligned} \Sigma(0.004, 0.8) &\equiv \int_{0.004}^{0.8} \frac{dx}{x} (F_2^p - F_2^n) \\ &= 0.227 \pm 0.007(\text{stat}) \pm 0.014(\text{syst}) \end{aligned} \quad (1)$$

at  $Q^2 = 4 \text{ GeV}^2$ . This is to be compared with the Gottfried sum rule [9]

$$\begin{aligned} I_{\text{GSR}} &= \Sigma(0, 1) \\ &\equiv \int_0^1 \frac{dx}{x} (F_2^p - F_2^n) \\ &= \frac{1}{3} \int_0^1 dx (u_V - d_V) + \frac{2}{3} \int_0^1 dx (\bar{u} - \bar{d}) \\ &= \frac{1}{3} \quad \text{if } \bar{u} = \bar{d} \text{ is assumed.} \end{aligned} \quad (2)$$

Here  $u(x, Q^2)$  has been expressed as the sum of valence and sea distributions:  $u = u_V + u_S$  and  $\bar{u} = u_S$ , and similarly for  $d(x, Q^2)$ . A straightforward comparison of (1) and (2) would imply that  $\bar{d} > \bar{u}$ , and indeed from the lack of Regge  $f - A_2$  exchange degeneracy we would

expect a difference behaving as

$$(\bar{d} - \bar{u}) \propto x^{-\alpha_R} \quad (3)$$

at small  $x$ , where the Regge intercept  $\alpha_R \simeq 0.5$ . Thus the second reason why it is timely to repeat the global structure function analysis is the necessity to relax the  $\bar{u} = \bar{d}$  assumption and to explore the effect of incorporating a flavor-breaking behavior of the type shown in (3) in the starting sea-quark distributions.

It is relevant to ask how our previous analyses [7, 10] with  $\bar{u} = \bar{d}$  were able to accommodate the Gottfried sum-rule measurement, or rather the precise NMC measurements of  $F_2^n/F_2^p$  at small  $x$ . We indeed found that parton distributions with  $\bar{u} = \bar{d}$  can be made consistent with the NMC measurements (and all other data) provided that the  $u$  and  $d$  valence distributions have a significantly different small- $x$  behavior. For example, the small- $x$  behavior of the Kwiecinski-Martin-Roberts-Stirling set  $B_0$  [KMRS( $B_0$ )] valence partons at  $Q^2 = 4 \text{ GeV}^2$  is [7]

$$x(u_V + d_V) = 0.42x^{0.27}(1 + 8.1x^{0.5} + \dots), \quad (4)$$

$$xd_V = 1.49x^{0.61}(1 + 1.1x^{0.5} + \dots). \quad (5)$$

The difference in the leading- $x^\delta$  behavior is able to give a significant contribution to  $\Sigma(0, 0.004)$  to enable the Gottfried sum rule to be satisfied. Note that in the region of the data,  $x \gtrsim 0.07$ , the second term in (4) is dominant which leads to an effective power of  $x$  much closer to that shown in (5). Although the resulting description of the data is satisfactory we see that it is obtained at the expense of a somewhat contrived behavior of the valence distributions at small  $x$ . Before the arrival of the new NMC and CCFR data, we had, for this reason, explored global fits which incorporated a behavior of the type shown in (3) and found an equally acceptable description of the data, or rather a slightly improved description with a smaller number of free parameters since all the  $x^\delta$  behaviors in (3), (4), and (5) were fixed assuming that the Regge meson intercepts have  $\alpha_R = 0.5$ . However, instead of presenting these sets of partons, we have waited until the new data became available so as to be able to incorporate them into the analysis. We are therefore able to give a more comprehensive and much improved structure function analysis.

The paper is organized as follows. In Sec. II we describe how we perform the analysis of the deep-inelastic and related data. We introduce the parametric forms of the input  $x$  distributions, allowing for the possibility that the  $u$  and  $d$  sea-quark distributions are no longer equal. Section III describes three different types of global fit to the data which allow (i) a comparison between a set of partons with  $\bar{u} = \bar{d}$  with one with  $\bar{u} \neq \bar{d}$  and (ii) a comparison between sets with singular and nonsingular gluons (and sea quarks). The incorporation of the new data, particularly for  $x \lesssim 0.1$ , significantly modifies the distributions at small  $x$  from the values obtained in earlier analyses. In Sec. IV we study the consequences of the new distributions. We first discuss the effect on the Gottfried sum rule and then we investigate in some detail  $W$ ,  $Z$ , and Drell-Yan production. We find  $p\bar{p}$  collider data

for these latter processes can provide tight constraints on the parton distributions. We conclude Sec. IV with predictions for the behavior of structure functions that will be measured at HERA. Finally, in Sec. V, we give our conclusions.

## II. FITTING PROCEDURE

The experimental measurements of the  $F_2$  structure function for deep-inelastic scattering of muon beams on hydrogen and deuterium targets have been dominated by the classic data from European Muon Collaboration (EMC) [11] and BCDMS [12]. The considerable discrepancies between the two sets of data have, as shown in [13], to a large extent disappeared after adjustments of the relative normalization and use of consistent assumptions for  $R = \sigma_L/\sigma_T$ . There is a small residual  $x$ -dependent discrepancy, which new NMC data appear to resolve in favor of BCDMS. Before the advent of the NMC data, the (BCDMS) data reached down to values of  $x$  as low as  $x \approx 0.07$  for  $Q^2 \gtrsim 5 \text{ GeV}^2$  and this provided the final point for parton distributions to latch on to before extrapolating out into the HERA territory of really small  $x$ . In our previous analysis [7] we obtained two such sets of parton distributions, KMRS  $B_0$  and  $B_-$ , which although giving almost identical descriptions of the data, extrapolate differently into the very small- $x$  region. These sets of partons have been widely used to predict various structure functions and hadronic cross sections at small  $x$  and over a wide range of  $Q^2$ .

In Fig. 1 we show the results of the KMRS  $B_0/B_-$  fits compared with new (preliminary [14])  $F_2$  data from NMC [4]. It is clear that in the low- $x$  region opened up by the NMC (extending down to  $x \approx 0.0125$ ) the data lie consistently *above* the old fits. In this paper we carry out a fresh analysis incorporating the new data of the NMC together with new data on  $\nu N$  structure functions from CCFR [5] and introducing new features into the phenomenological analysis itself. As a result we produce

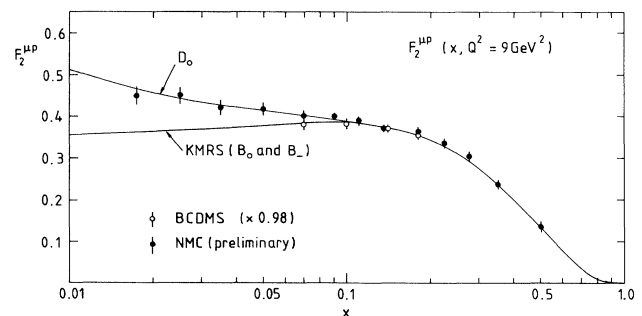


FIG. 1. The values of  $F_2^{\mu p}(x, Q^2)$  as a function of  $x$  at  $Q^2 = 9 \text{ GeV}^2$  obtained by interpolating the structure function measurements of the BCDMS Collaboration [12] and NMC [4]. The upper curve corresponds to the  $D_0$  set of partons obtained in the present global analysis and the lower curve to the earlier KMRS sets of partons obtained in analyses [7] before the NMC data were available.

new sets of parton distributions which reflect the new information and therefore provide a much improved basis for future phenomenology. Figure 1 also shows the result of the new fits, the improvement indicating a marked rise in the predictions at even smaller  $x$ . The comparison of the two curves emphasizes how heavily the extrapolation to small  $x$  of the old distributions hung upon the BCDMS measurement at  $x = 0.07$ . The new data are already higher even at this  $x$  value.

We begin with some details of the procedure used in our next-to-leading order (NLO) QCD analysis of deep-inelastic data. The parametrization of the various parton distributions at  $Q_0^2 = 4 \text{ GeV}^2$  follows the form used in our previous analysis [7]. The gluon distribution  $xg(x, Q_0^2)$  is allowed to be either finite at  $x=0$  (the fits carrying a subscript 0) or singular, i.e., roughly  $xg(x) \sim x^{-1/2}$  as  $x \rightarrow 0$  (the subscript  $-$  being used for this case). So we write

$$xg(x, Q_0^2) = A_g x^{\delta_g} (1 + \gamma_g x) (1 - x)^{\eta_g} \quad (6)$$

and, for the choices  $\delta_g = 0, -\frac{1}{2}$ , the parameters  $\gamma_g, \eta_g$  are determined by the prompt-photon ( $pp \rightarrow \gamma x$ ) data of WA70 [16]. Thus in this way we shall obtain new sets of partons  $S_0$  and  $D_0$  (defined below) replacing KMRS [7] set  $B_0$ , and set  $D_-$  replacing KMRS set  $B_-$ .

The total sea-quark distribution at  $Q_0^2$  is parametrized in the form

$$\begin{aligned} xS &\equiv 2x (\bar{u} + \bar{d} + \bar{s}) \\ &= A_S x^{\delta_s} (1 + \epsilon_S x^{1/2} + \gamma_S x) (1 - x)^{\eta_S} \end{aligned} \quad (7)$$

reflecting the fact that the sea quarks are expected to have the same leading  $x \rightarrow 0$  behavior as the gluon. The charm-quark distributions are generated, as usual, through the evolution equations taking  $c(x, Q_0^2) = 0$  [17]. The strange sea is known to be roughly half the  $\bar{u}$  or  $\bar{d}$  sea [18], so we take  $\bar{s} = \frac{1}{4}(\bar{u} + \bar{d})$  at  $Q_0^2$ . As discussed in the Introduction a new feature of the analysis is the freedom for the  $\bar{u}$  and  $\bar{d}$  distributions to differ. The parametrizations of the sea-quark distributions at  $Q_0^2$  are therefore written as

$$\begin{aligned} 2\bar{s} &= 0.2 S, \\ 2\bar{d} &= 0.4 S + \Delta, \\ 2\bar{u} &= 0.4 S - \Delta, \end{aligned} \quad (8)$$

with

$$x\Delta \equiv x (\bar{d} - \bar{u}) = A_\Delta x^{\eta_\Delta} (1 - x)^{\eta_S}. \quad (9)$$

The value of the Gottfried sum rule (2) is then given by

$$I_{\text{GSR}} = \frac{1}{3} - \frac{2}{3} A_\Delta B(\eta_\Delta, 1 + \eta_S). \quad (10)$$

We actually carry out fits with  $A_\Delta = 0$  (labeled as S for  $\bar{u}$  and  $\bar{d}$  the *same*) and with  $A_\Delta \neq 0$  (labeled as D for  $\bar{u}$  and  $\bar{d}$  *different*). We can thus study the effect of allowing  $\bar{u} \neq \bar{d}$  by comparing fit  $S_0$  with fit  $D_0$ , and study the effects of a singular gluon by comparing fit  $D_0$  with fit  $D_-$ .

The distribution  $\Delta(x)$  is thus a flavor nonsinglet and we would expect, by Regge behavior,  $\eta_\Delta \approx \frac{1}{2}$ . The other nonsinglet distributions are the valence quarks parametrized by

$$\begin{aligned} x[u_V(x) + d_V(x)] \\ = A_{ud} x^{\eta_1} (1 - x)^{\eta_2} (1 + \epsilon_{ud} x^{1/2} + \gamma_{ud} x), \end{aligned} \quad (11)$$

$$x d_V = A_d x^{\eta_3} (1 - x)^{\eta_4} (1 + \epsilon_d x^{1/2} + \gamma_d x),$$

with  $A_{ud}$  and  $A_d$  fixed in terms of the  $\eta$ 's,  $\epsilon$ 's, and  $\gamma$ 's to give the correct number of valence quarks.

As is well known, the singular gluon ( $\delta_g = -\frac{1}{2}$ ), as  $x$  decreases, ultimately leads to significant gluon-gluon interactions which "soften" this behavior. These shadowing effects are the center of intense study and will be one of the major subjects of investigation at HERA. We follow precisely the same procedure detailed in KMRS [7] and introduce two types of modification to take account of this gluon recombination. First the small- $x$  behavior of the gluon distribution (and the sea distribution) is altered at  $Q_0^2$ :

$$xg(x, Q_0^2) \rightarrow xg(x, Q_0^2) \left\{ 1 + \frac{\theta(x_0 - x)[C(x)x^{-1/2} - C(x_0)x_0^{-1/2}]}{xg_{\text{sat}}(x, Q_0^2)} \right\}^{-1}, \quad (12)$$

where the unmodified distribution  $xg(x) \sim C(x)x^{-1/2}$ , and where

$$xg_{\text{sat}}(x, Q^2) = 16R^2 Q^2 / 27\pi\alpha_s(Q^2) \quad (13)$$

is the value of the gluon which would saturate the unitarity limit. The form of Eq. (12), which leads to shadowing corrections only for  $x < x_0$ , is justified in Ref. [7]. Shadowing effects are important only for very small  $x$  and we find it reasonable to choose  $x_0 = 10^{-2}$ . Thus it is sufficient and convenient to impose the corrections after fitting to the data which all lie in the region  $x > x_0 = 10^{-2}$ . As in [7] we consider two values of the radius parameter

$R$  which characterizes the nature of the coupling of the gluon ladder to the proton or, to put it another way, which describes how the gluons are distributed within the proton. We take  $R = 5 \text{ GeV}^{-1}$  ( $\sim$  proton radius), which corresponds to the gluons being uniformly spread throughout the proton and then repeat the calculation with  $R = 2 \text{ GeV}^{-1}$  to illustrate the effect of concentrating the gluons in "hot spots" within the proton. This latter picture represents a rather extreme limit of the shadowing mechanism—in practice it leads to a suppression of the singular gluon to the extent that it is then not far from the finite gluon solution ( $\delta_g = 0$ ). The second modification due to shadowing is in the evolution of the

gluon and sea distributions. A nonlinear term is incorporated into the evolution equations whose size is governed by the shadowing radius,

$$\begin{aligned} \frac{\partial(xg(x, q^2))}{\partial \ln Q^2} &\rightarrow \frac{\partial(xg(x, q^2))}{\partial \ln Q^2} \\ &- \frac{81\alpha_s^2(Q^2)}{16R^2Q^2} \int_x^{x_0} \frac{dx'}{x'} [x'g(x', Q^2)]^2 \end{aligned} \quad (14)$$

and an analogous, but more complicated, modification for the evolution of the sea quark. The details are to be found in Ref. [7]. Again the modifications are relevant only for  $x < x_0$ . However the suppression it causes for  $x < x_0$  will lead to a small violation of the momentum sum rule, which we restore by a simple renormalization of the distributions.

The deep-inelastic data that are used in the global analysis are (i) the new, but preliminary [14], NMC data on  $F_2^{\mu p}$  and  $F_2^{\mu D}$  [4], (ii) BCDMS data on  $F_2^{\mu p}$  and  $F_2^{\mu D}$  [12], (iii) data on  $F_2^{\mu n}/F_2^{\mu p}$  from NMC [19], BCDMS [20], and EMC [21], (iv) the wideband beam neutrino data from CCFR [5] and CDHSW [6] on  $F_2^{\nu N}$  and  $xF_3^{\nu N}$ .

In addition to these deep-inelastic data we also incorporate (v) WA70 data on prompt photon production [16], (vi) E605 data on Drell-Yan production [22], and (vii) constraints from  $W$  and  $Z$  production at  $p\bar{p}$  colliders.

The relative importance of the constraints imposed by the various sets of data (i) – (vi) is described in previous work (Harriman *et al.* [1]). The implications of the new  $W$  and  $Z$  data are discussed in detail in Sec. IV C. The new input in (iv) are the preliminary wideband beam neutrino data from CCFR which show a significant deviation from the CDHSW wideband beam data. As in our previous analyses which include data taken from experiments using heavy nuclear targets, we correct for the nuclear distortion to the structure functions. The correction is based on precise measurements of the ratio of iron to deuterium cross sections. The numerical values at the  $x$  values of the CCFR data are listed in Table I. In addition to the parameters describing the starting parton distributions in Eqs. (6)–(11) we also have  $\Lambda_{\overline{\text{MS}}}$  and the relative normalizations of the data sets, where  $\overline{\text{MS}}$  denotes the modified minimal subtraction scheme. As shown in Ref. [24], when compared to the SLAC data over the full- $Q^2$  range, the BCDMS data require a 2% shift down (whereas the EMC data need to be shifted up by  $\sim 7\%$ ). We find, as a result of our new fits, that this shift remains for the BCDMS relative to the NMC. We find that a larger shift is required for the CCFR data. In summary, relative to the SLAC data, the renormalizations of the BCDMS, NMC, CDHSW, and CCFR data sets are found to be 0.98, 1.00, 1.00, and 0.94, respectively. More accurate renormalizations must await the final experimental analyses.

### III. FITS TO DATA

As mentioned above, we perform three different types of fit to the data to explore first the effect of allowing  $\bar{u}$  to

TABLE I. The  $x$ -dependent correction factor which is applied to the neutrino structure functions to take account of the distortion due to nuclear effects (EMC effect). This correction is based on a parametrization of the experimental values for the iron/deuterium structure function ratios compiled in Ref. [23].

$x$	Correction factor
0.045	0.965
0.080	1.015
0.150	1.026
0.250	1.015
0.350	0.958
0.450	0.916
0.550	0.883
0.650	0.855

be different from  $d$  and, second, the difference between starting the evolution with a singular and nonsingular gluon. The resulting three sets of partons are labeled (i)  $S_0$  :  $xg(x, Q_0^2) \sim \text{const}$  as  $x \rightarrow 0$ , and  $\bar{u} = \bar{d}$ , (ii)  $D_0$  :  $xg(x, Q_0^2) \sim \text{const}$  as  $x \rightarrow 0$ , and  $\bar{u} < \bar{d}$ , and (iii)  $D_-$  :  $xg(x, Q_0^2) \sim x^{-1/2}$  as  $x \rightarrow 0$ , and  $\bar{u} < \bar{d}$ . We also study the effect of shadowing on the small- $x$  behavior of the  $D_-$  distributions, according to Eqs. (12)–(14) with both  $R = 5 \text{ GeV}^{-1}$  and  $2 \text{ GeV}^{-1}$ .

The values of the parameters obtained in the three fits are listed in Table II. All three resulted in a value of  $\Lambda$  of QCD:

$$\Lambda_{\overline{\text{MS}}}(n_f = 4) = 215 \pm 60 \text{ MeV}, \quad (15)$$

where the error includes the uncertainty due to scale dependence [25]. This corresponds to

$$\alpha_s(M_Z) = 0.111^{+0.004}_{-0.005}. \quad (16)$$

The inclusion of the new data has thus slightly raised the prediction for the strong coupling from our previous value [25] of

$$\Lambda_{\overline{\text{MS}}}(n_f = 4) = 190 \pm 80 \text{ MeV}$$

or

$$\alpha_s(M_Z) = 0.109^{+0.007}_{-0.008}. \quad (17)$$

The value of the strong coupling, shown in (15) or (16), is in excellent agreement with an independent determination [26] using a BCDMS and SLAC subset of the deep-inelastic data. It is also in agreement with the determination from the CERN  $e^+e^-$  collider LEP experiments [27] based on event topology:

$$\alpha_s(M_Z) = 0.120 \pm 0.007. \quad (18)$$

Indeed the accuracy of the deep-inelastic determination

of  $\alpha_s(M_Z)$  is comparable to that presently available at LEP.

The values of the  $x$  exponents of the valence quarks in the  $S_0$  fit,  $\eta_1 = 0.26$  and  $\eta_3 = 0.78$ , contrive to make  $x(u_V - d_V)$  fall slowly as  $x \rightarrow 0$  and so be consistent with NMC data on  $F_2^p - F_2^n$  as well as the  $\frac{1}{3}$  value of the integral  $I_{GSR} \equiv \Sigma(0, 1)$  of Eq. (2). In the D-type fits, the value of  $\eta_\Delta$  always came close to  $\frac{1}{2}$  as expected.

Now we turn to the resulting comparison with the data. Figure 2 shows the new NMC (preliminary [14]) and the BCDMS data ( $\times 0.98$ ) for  $F_2^{\mu p}$ . It is clear that we have obtained a fit which is able to describe the new data while still maintaining success in fitting the larger  $x$  region of the BCDMS data. The same is true for the deuterium data shown in Fig. 3. The dashed curves in Fig. 2(a)

TABLE II. The upper portion of the table lists the values of the parameters of the parton distributions found in the three types of optimum fit to the data. For sets  $S_0$  and  $D_0$  we fix the gluon exponent  $\delta_g = 0$ , and for  $D_-$  we set  $\delta_g = -\frac{1}{2}$ . We also list the value of the Gottfried sum rule  $I_{GSR}$  and the percentage of the proton's momentum carried by each type of parton at  $Q_0^2 = 4 \text{ GeV}^2$ . Finally, we show the values of the  $K'$  factor which are required to achieve agreement with the Drell-Yan data of E605 [22].

	$S_0$	$D_0$	$D_-$
$\Lambda_{\overline{MS}}(n_f = 4) \text{ (MeV)}$	215	215	215
<b>Glue</b>			
$\delta_g$	0	0	-0.5
$\gamma_g$	0	0	12.0
$A_g$	2.72	2.72	0.315
$\eta_g$	5.1	5.1	5.1
<b>Valence</b>			
$\eta_1$	0.26	0.45	0.46
$\eta_2$	3.82	3.91	3.84
$\eta_3$	0.78	0.35	0.24
$\eta_4$	4.57	4.66	4.59
$\epsilon_{ud}$	14.4	2.46	3.16
$\gamma_{ud}$	16.99	3.32	2.05
$\epsilon_d$	-0.87	11.4	34.4
$\gamma_d$	0.82	3.0	9.0
<b>Sea</b>			
$\eta_S$	10	10	6.5
$A_S$	1.87	1.93	0.054
$\gamma_S$	6.22	7.38	-3.28
$\epsilon_S$	-2.21	-2.68	19.5
$A_\Delta$	0	0.163	0.144
$\eta_\Delta$	-	0.45	0.46
Drell-Yan $K'$ factor	1.15	1.12	1.09
$I_{GSR}$	0.333	0.260	0.259
<b>Momentum % at <math>Q_0^2 = 4 \text{ GeV}^2</math></b>			
Glue	44.6	44.6	44.0
$u_{val}$	27.6	28.0	28.2
$d_{val}$	11.7	11.1	10.9
$u_{sea}$	6.4	6.1	6.1
$d_{sea}$	6.4	6.9	7.4
$s_{sea}$	3.2	3.2	3.4

show that the predictions of the KMRS partons [7], extrapolated from fits to the BCDMS data with  $x \gtrsim 0.07$ , considerably undershoot the new  $F_2^{\mu p}$  data at smaller  $x$ . The situation is also well illustrated by Fig. 1.

In Fig. 4 the data on  $F_2^{\mu n}/F_2^{\mu p}$  from NMC are compared with the three fits. Although EMC and BCDMS data are also included in the fits, it is the very precise

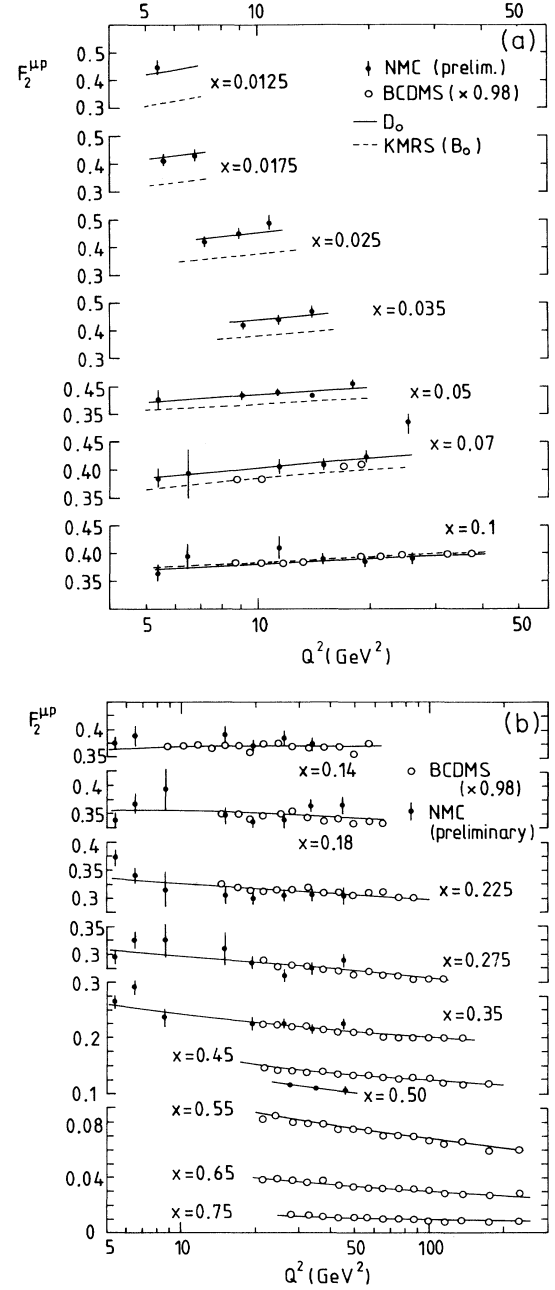


FIG. 2. The continuous curves show the description of the BCDMS [12] and NMC [4] measurements of the  $F_2^{\mu p}(x, Q^2)$  structure function by the  $D_0$  set of partons. The dashed curves in diagram (a) show the predictions obtained from the KMRS (set  $B_0$ ) parton distributions [7].

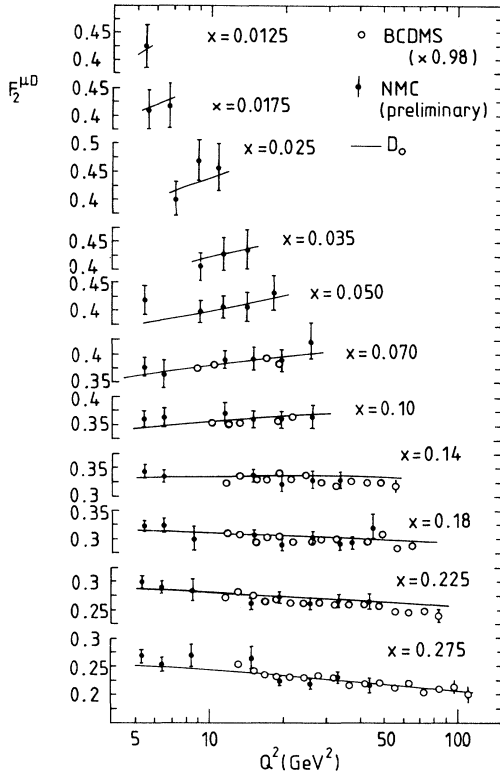


FIG. 3. The description of the BCDMS [12] and NMC [4] measurements of the  $F_2^{\mu D}(x, Q^2)$  structure function given by the  $D_0$  set of partons. Sets  $S_0$  and  $D_-$  give almost identical fits.

NMC data which tend to drive the resulting parameters. The  $S_0$  fit, like the old  $B_0$  fit of KMRS, needs to juggle with the exponents  $\eta_1$  and  $\eta_3$ , which govern the small- $x$  region of the valence quarks, in order to agree with the very small- $x$  points. In contrast, the extra freedom of having  $\bar{u} \neq \bar{d}$  allows the parameters  $\eta_1$ ,  $\eta_3$ , and  $\eta_\Delta$  to be all different but the fits prefer to have all three values close to  $\frac{1}{2}$ . The extraction of the  $n/p$  ratio from experiment requires a nuclear correction for the deuteron and since the binding is weak this correction, certainly at small  $x$ , is bound to be small. However at small  $x$ , our fits are sensitive to the small quantity  $\rho = [1 - F_2^{\mu n}/F_2^{\mu p}]$  which is just  $2[1 - F_2^{\mu D}/F_2^{\mu p}]$  where  $D \equiv \frac{1}{2}(p+n)$ . A small fractional charge  $\delta$  to  $D$  leads to an absolute change  $-2\delta$  to  $\rho$  and so any uncertainty in the deuteron correction at small  $x$  implies significant uncertainty in the parameters describing the small- $x$  behavior.

Figures 5 and 6 show the new (preliminary)  $\nu N$  data on  $F_2$  and  $xF_3$  from CCFR [5] compared with the CDHSW data [6] (also obtained using a wideband neutrino beam). The continuous curves are our fit to the new CCFR data. The renormalization of the CCFR data by 6% relative to the CDHSW data is important in obtaining acceptable fits. The dashed curves in Figs. 5 and 6 show, for comparison, the KMRS fits obtained in an earlier global analysis [7] which included only the neutrino data of CDHSW.

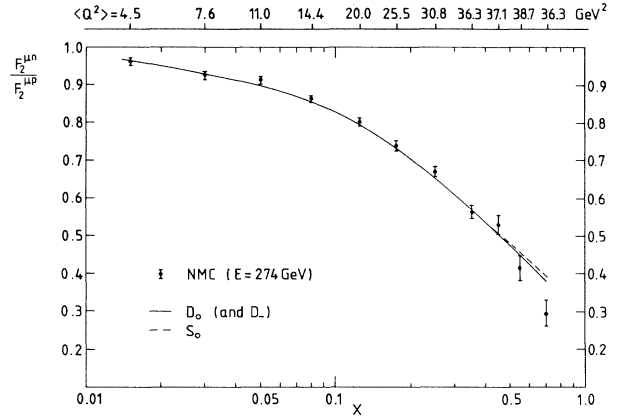


FIG. 4. The description of the NMC data [19] for the structure function ratio  $F_2^{\mu n}/F_2^{\mu p}$  given by the  $D_0$ ,  $S_0$ , and  $D_-$  sets of parton distributions. The mean  $Q^2$  of the data varies with  $x$  as shown by the uppermost scale. The curves take this  $Q^2$  dependence into account.

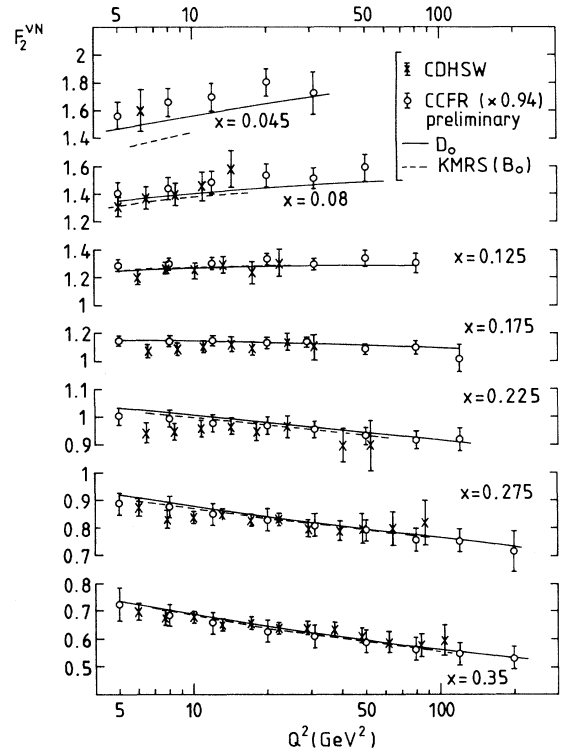


FIG. 5. The continuous curves show the description of the CDHSW [6] and new preliminary CCFR [5] measurements of the  $F_2^{\nu N}(x, Q^2)$  structure function by the  $D_0$  set of partons. All data are shown after correction for the nuclear modification to the structure function. The dashed curves, corresponding to KMRS (set  $B_0$ ) parton distributions [7], were obtained in an earlier global analysis which included only the CDHSW data.

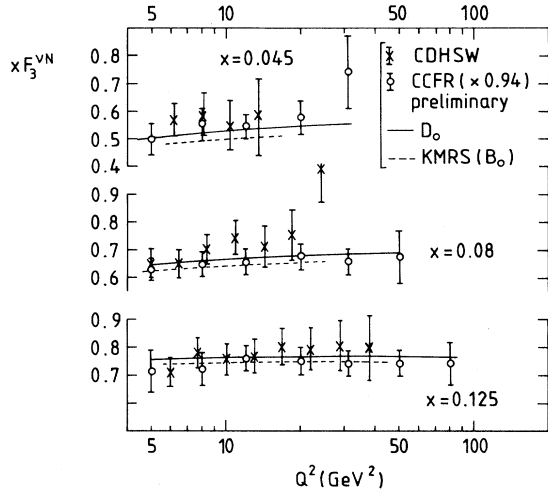


FIG. 6. As for Fig. 5 but for the structure function  $x F_3^{\nu N}(x, Q^2)$ .

One can see the improved quality of the new fit, even with the CDHSW data alone.

A summary of the quality of the description of the deep-inelastic data by each of the three sets of partons is given in Table III. There we tabulate the contribution to the total  $\chi^2$  arising from the individual subsets of data.

Figure 7 shows our description of the WA70 [16] prompt photon production data,  $pp \rightarrow \gamma X$ . Here the

TABLE III. Description of the deep-inelastic data for the three sets of partons shown in terms of  $\chi^2$ .

Measurement		No. of data	$\chi^2$		
			D <sub>0</sub>	S <sub>0</sub>	D <sub>-</sub>
BCDMS	$F_2^{\mu p}$	142	153	144	148
NMC <sup>a</sup>	$F_2^{\mu p}$	73	100	101	100
NMC <sup>a</sup>	$F_2^{\mu D}$	73	78	83	78
EMC	$F_2^n / F_2^p$	10	3	3	3
BCDMS	$F_2^n / F_2^p$	11	5	7	5
NMC	$F_2^n / F_2^p$	11	17	20	17
CDHSW	$F_2^{\nu N}$	84	59	53	60
CDHSW	$x F_3^{\nu N}$	94	53	56	56
CCFR <sup>a</sup>	$F_2^{\nu N}$	81	36	34	37
CCFR <sup>a</sup>	$x F_3^{\nu N}$	79	25	30	25

<sup>a</sup>The NMC and CCFR data that we use are preliminary; also we have enlarged the errors on the CCFR data to allow, *inter alia*, for the uncertainty in the heavy target correction. However very recently the final NMC data (July 1992 [15]) and CCFR data (August 1992) have been released. These data are essentially identical to the data that we have used, apart from our overestimation of the errors on the CCFR values. Indeed our solution D<sub>0</sub>, for example, if compared to the new data would yield  $\chi^2/\text{No. of data} = 99/74, 72/74, 70/77, 56/77$  for NMC ( $F_2^{\mu p}, F_2^{\mu D}$ ) and CCFR ( $F_2^{\nu N}, x F_3^{\nu N}$ ). That is an improved description of the NMC data and an excellent description of the CCFR data.

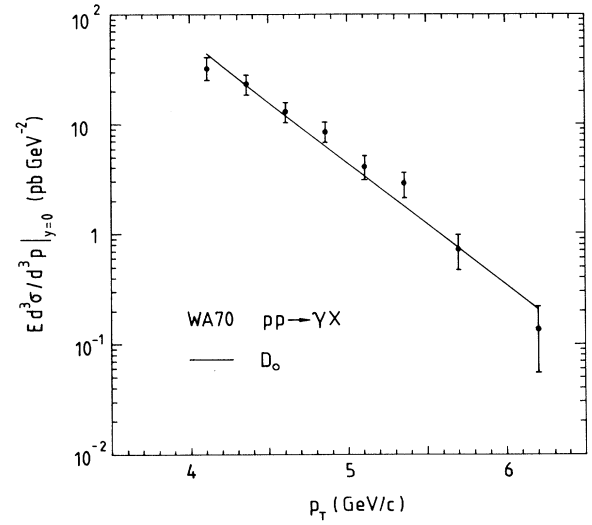


FIG. 7. Data on the prompt photon transverse momentum distribution in  $pp$  collisions at  $\sqrt{s} = 23$  GeV from the WA70 Collaboration [16] (corrected to  $y = 0$  [28]), together with the fit from the D<sub>0</sub> set of partons.

dominant QCD subprocess is  $qg \rightarrow \gamma q$  and these data pin down the gluon distribution in the region  $x \sim 0.4$ .

#### IV. IMPLICATIONS AND CONSEQUENCES

The continuous curves in Fig. 8 show the D<sub>0</sub> set of parton distributions as a function of  $x$  at  $Q^2 = 20$  GeV<sup>2</sup>. For comparison we also show the distributions of the B<sub>0</sub> set obtained in the earlier KMRS analysis. Although the agreement is excellent for  $x \gtrsim 0.1$ , we see the quark distributions differ significantly at small  $x$ , reflecting the influence of the new small- $x$  data. Likewise the quark distributions of solutions S<sub>0</sub> and D<sub>-</sub> are also considerably above those of the B<sub>0</sub> set at small  $x$ . In this section we

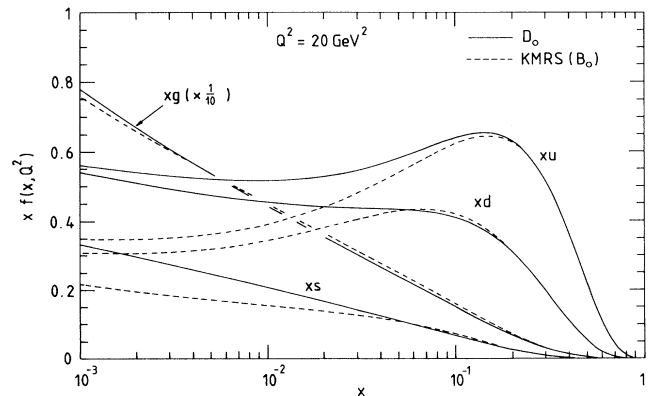


FIG. 8. Parton distributions for the  $u$ ,  $d$ ,  $s$  quarks and the gluon from the D<sub>0</sub> fit (continuous curves) compared with the earlier B<sub>0</sub> fit [7] (dashed curves).

explore the consequences of the new solutions and discuss future measurements which may be able to distinguish between the differing small- $x$  behaviors. We begin by looking again at the Gottfried sum rule.

### A. Gottfried sum rule

As discussed in Sec. I, one of the motivations for relaxing the  $\bar{u} = \bar{d}$  assumption of our previous fits was to better accommodate the lower value of the Gottfried sum rule indicated by the NMC measurement [8]. Although fits with  $\bar{u} = \bar{d}$  could successfully describe the integrand  $F_2^{p-n} \equiv F_2^p - F_2^n$  [10] the exponents  $\eta_1, \eta_3$  are found to have rather unphysical values. However there is no strong theoretical justification for maintaining the equality  $\bar{u} = \bar{d}$ . Indeed, as mentioned in Secs. II and III, choosing  $\bar{u} \neq \bar{d}$  results in a more "natural" situation where the values of the exponents  $\eta_1, \eta_3$ , and  $\eta_\Delta$  all cluster around the Regge expectation of  $\frac{1}{2}$ . In Fig. 9 we show the values of  $F_2^{p-n}$  from our fits at  $Q^2 = 7 \text{ GeV}^2$ . As expected, the D-type fits drop significantly faster at small  $x$  than the  $S_0$  fit. The experimental estimates of the difference  $F_2^p - F_2^n$  and of the sum rule published by the NMC [8] were based on combining their own measurements of the  $n/p$  ratio with a fit to  $F_2^D$  from other experiments:

$$F_2^{p-n}(x) = 2 F_2^D(x) \frac{1 - F_2^n/F_2^p}{1 + F_2^n/F_2^p}. \quad (19)$$

This fit does not reflect the new information at small  $x$  and a more recent, but preliminary [14], estimate from

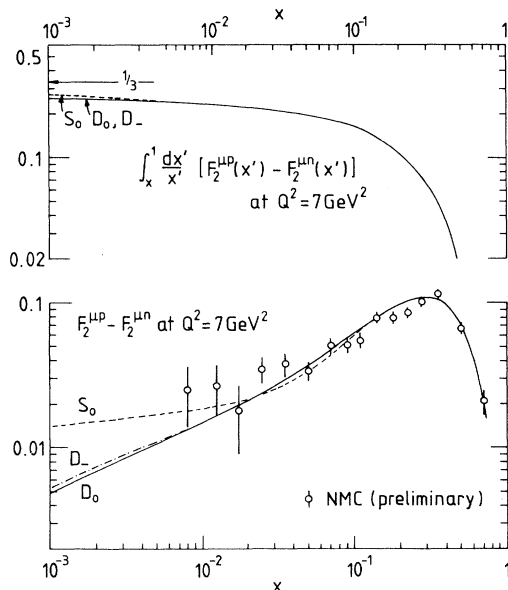


FIG. 9. The upper curves give the accumulated contribution,  $\Sigma(x, 1)$  of Eq. (1), to the Gottfried sum rule as a function of  $x$ , the lower limit of integration. Predictions are shown for sets  $S_0, D_0$ , and  $D_-$  of partons. The lower curves compare the integrand,  $F_2^{\mu p} - F_2^{\mu n}$ , with preliminary [14] estimates by NMC [4].

the NMC [4], obtained directly from their new structure functions is shown by the data points in Fig. 9.

Also shown in Fig. 9 are the resulting estimates of the integral

$$\Sigma(0, x) = \int_x^1 \frac{dx'}{x'} F_2^{p-n}(x'). \quad (20)$$

At  $x = 10^{-3}$  all three fits give values around 0.26-0.27 though the "asymptotic" values for the S- and D-type fits are quite different (see Table II). It is hard to say precisely how the experimental estimate of the Gottfried sum rule will be modified as a result of the new data at small  $x$ . A recent study [29] of possible nuclear corrections to  $F_2^D$  demonstrated that changes of the order of 3% to  $F_2^D$  could lead to changes in the value of  $\Sigma(0, 1)$  by nearly 40%. On the other hand explicit estimates [30] of shadowing corrections to deuterium indicate effects well under 2% in the range of the NMC data.

In Fig. 10 we show the resulting  $u$  and  $d$  sea-quark distributions and their difference at two widely different values of  $Q^2$ . The difference  $x\Delta(x)$  reaches its peak around  $x = 0.04$ . The value of  $x\bar{u} = x\bar{d}$  for the  $S_0$  fit is sandwiched between the values of  $x\bar{u}$  and  $x\bar{d}$  for the  $D_0$  fit.

### B. $Q^2$ dependence of structure functions

One of the interesting new pieces of information in this analysis is the new (preliminary) set of wideband neutrino data from CCFR [5]. Perhaps the most signif-

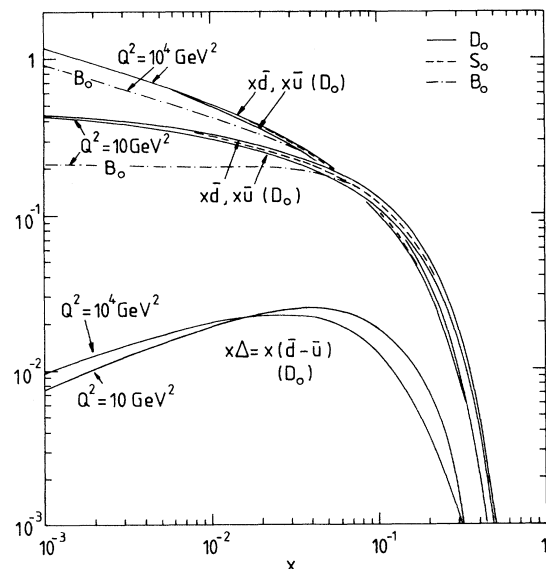


FIG. 10. The behavior of the sea-quark distributions as a function of  $x$  for  $Q^2 = 10 \text{ GeV}^2$  and for  $Q^2 = 10^4 \text{ GeV}^2$ . The continuous curves correspond to the  $D_0$  set of partons (with  $\bar{u}$  different from  $\bar{d}$ ) and the dashed curves are for  $S_0$  partons (with  $\bar{u} = \bar{d}$ ). For comparison the dot-dashed curves show the  $x\bar{u} = x\bar{d}$  distributions of the KMRS( $B_0$ ) set of partons [7]. The lower two curves show the difference  $x\Delta \equiv x(\bar{d} - \bar{u})$  found for the  $D_0$  set for  $Q^2 = 10$  and  $10^4 \text{ GeV}^2$ .



icant feature is the difference in the  $Q^2$  behavior of the two data sets. The discrepancy may not be immediately obvious from Fig. 5 but if we compute the derivative  $d \ln F_2(x, Q^2)/d \ln Q^2$  at fixed- $x$  values the difference becomes plain to see. Figure 11 shows the values of this derivative for each data set compared with the resulting QCD prediction of this analysis. It is clear that the new data are more in line with the expectations of the theory. It is most important in making such a comparison that only data on the structure functions which fall in the range of validity of leading twist QCD, namely,  $Q^2 > 5 \text{ GeV}^2$  and  $W^2 > 10 \text{ GeV}^2$ , are used in computing the experimental values of the derivative. For example, removing the  $W^2$  cut modifies the large- $x$  points substantially. When the full CCFR data becomes available it will be interesting to see if the consistency with QCD continues out to large  $x$ . Such consistency is graphically demonstrated for the muon data in Fig. 12 where the small uncertainties in the BCDMS values of  $F_2$  allow a very precise determination of the derivatives. Again, these derivatives are computed from data satisfying the required cuts in  $Q^2$  and  $W^2$ . Because of these cuts the error on the NMC point at  $x = 0.5$  becomes very large.

### C. $W$ , $Z$ , and Drell-Yan hadroproduction

One of the most direct tests of parton distributions comes from "Drell-Yan"-type processes:  $q\bar{q} \rightarrow$

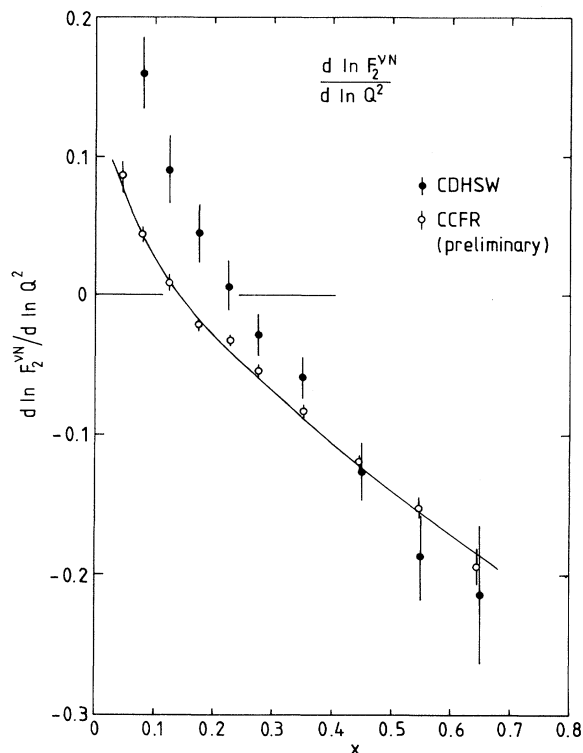


FIG. 11. The curve shows  $d \ln F_2^{\mu N} / d \ln Q^2$  calculated from set  $D_0$  of partons compared to the values obtained from CDHSW [6] and new preliminary CCFR [5] data.

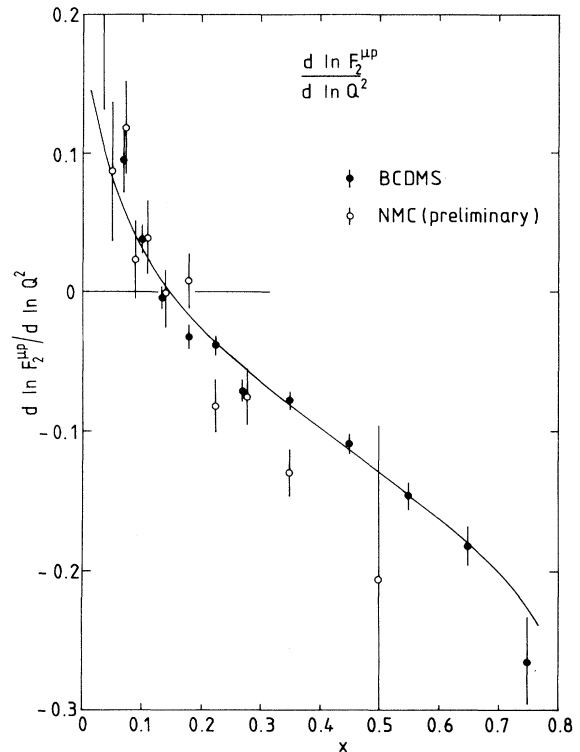


FIG. 12. The curve shows  $d \ln F_2^{\mu p} / d \ln Q^2$  calculated from set  $D_0$  of partons compared to the values obtained from BCDMS [12] and calculated from those new preliminary [14] NMC data [4] that satisfy our cuts (see text).

$W, Z, \gamma^* (\rightarrow l^+ l^-)$ . In fact we have already used the fixed target Drell-Yan dilepton data from E605 to constrain the sea distribution at medium to large- $x$  values. At the  $p\bar{p}$  colliders, on the other hand, the higher collision energies provide a probe of the quarks and antiquarks at smaller  $x$  values. In addition the dominant contributions to the cross sections come from the scattering of essentially the same "valence + sea" combinations that enter in the deep-inelastic scattering structure functions.

Since our main interest in the present study is the new information on the quark distributions in the  $0.01 - 0.1-x$  range, we address the question of whether  $W$ ,  $Z$ , or Drell-Yan (i.e., dilepton) cross sections measured in  $p\bar{p}$  collisions at  $\sqrt{s} = 630 \text{ GeV}$  and  $1.8 \text{ TeV}$  can provide independent information on the quark distributions. In what follows we will compare the predictions of the old and new sets for various electroweak cross sections measured at the  $p\bar{p}$  colliders. It will prove useful in understanding the differences between the predictions to refer back to the differences in the quark distributions themselves, illustrated in Fig. 8.

We can summarize the relevant collider phenomenology as follows.

- (i) The total cross section  $\sigma_W \equiv \sigma(p\bar{p} \rightarrow W + X)$  is sensitive to the  $u$  and  $d$  distributions around  $x \sim M_W/\sqrt{s}$ .
- (ii) The ratio of  $W$  to  $Z$  total cross sections  $R_\sigma \equiv \sigma_W/\sigma_Z$  is sensitive to the magnitude of the ratio of  $d$  and

$u$  quarks, just like the structure function ratio  $F_2^{\mu n}/F_2^{\mu p}$ .

(iii) The  $W \rightarrow$  charged lepton rapidity asymmetry

$$A(y) = \frac{d\sigma(l^+)/dy - d\sigma(l^-)/dy}{d\sigma(l^+)/dy + d\sigma(l^-)/dy} \quad (21)$$

is also sensitive to the  $d/u$  ratio, but more to the slope in  $x$  rather than the absolute magnitude [31].

(iv) The  $Z$  rapidity distribution at large  $y_Z$  probes the quark distributions at much smaller  $x \sim \exp(-y_Z)M_Z/\sqrt{s}$  than the total cross section.

(v) The lepton-pair cross section  $M^3 d\sigma/dM dy|_{y=0}$ , where  $M = M_{l+l^-}$  and  $y = y_{l+l^-}$ , is also sensitive to the (dominantly  $u$ ) quark distributions, and since the  $p\bar{p}$  collider experiments can in principle measure dimuon masses down to  $M = M_\Upsilon \sim 10$  GeV, this means significantly smaller  $x$  values than are probed by  $\sigma_W$  or  $\sigma_Z$ .

Figures 13–18 and Table IV show the predictions of the new parton sets  $S_0$ ,  $D_0$ , and  $D_-$  for all the above quantities, together with the measurements from the  $p\bar{p}$  collider experiments where available. For comparison, the predictions of the previous  $B_0$  set are also shown.

Figure 13 shows the total  $W$  and  $Z$  production cross sections times leptonic branching ratios as a function of the  $p\bar{p}$  collider energy  $\sqrt{s}$ , together with recent measurements from the UA2 [32] and Collider Detector at Fermilab (CDF) [33] collaborations. The theoretical pre-

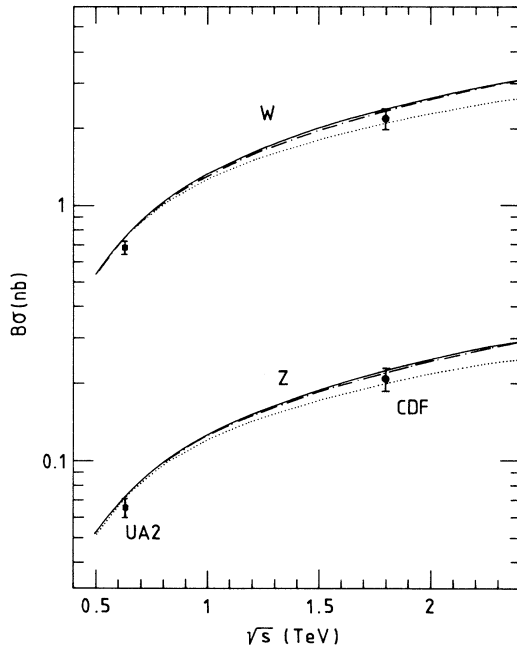


FIG. 13. Cross sections times leptonic branching ratios in  $p\bar{p}$  collisions as a function of  $\sqrt{s}$ . The curves are the theoretical predictions calculated to  $O(\alpha_s^2)$  in QCD, corresponding to the  $S_0$ ,  $D_0$  (continuous) and  $D_-$  (dash-dot) parton distributions. The prediction of set  $B_0$  (dotted) of Ref. [7] is shown for comparison. The data are from the UA2 [32] (squares) and CDF [33] (circles) collaborations, with statistical and systematic errors added in quadrature.

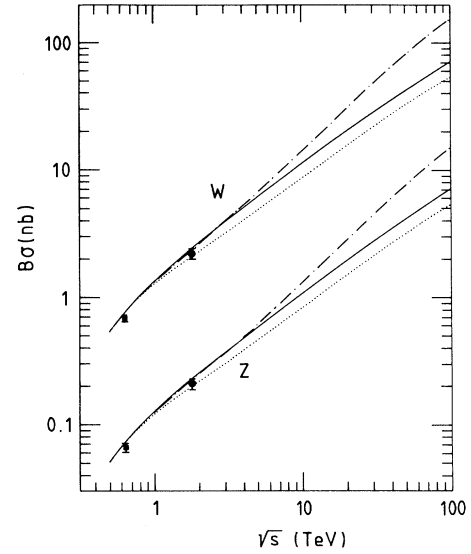


FIG. 14. As for Fig. 13, but for higher collision energies  $\sqrt{s}$ .

dictions are calculated to  $O(\alpha_s^2)$  in QCD perturbation theory, using the results of Hamberg *et al.* [34]. The renormalization and factorization scales are set equal to the weak-boson masses:  $Q = \mu = M_V$ , with  $M_W = 80.14$  GeV [35] and  $M_Z = 91.175$  GeV [36]. Values for the branching ratios

$$B(W \rightarrow e\nu) = 0.108, \quad B(Z \rightarrow e^+e^-) = 0.0336, \quad (22)$$

corresponding to three light neutrinos and  $m_t > M_W$ , are used. At 630 GeV the predictions are very similar, simply because at this value of  $x \sim M_W/\sqrt{s} \sim 0.13$  all

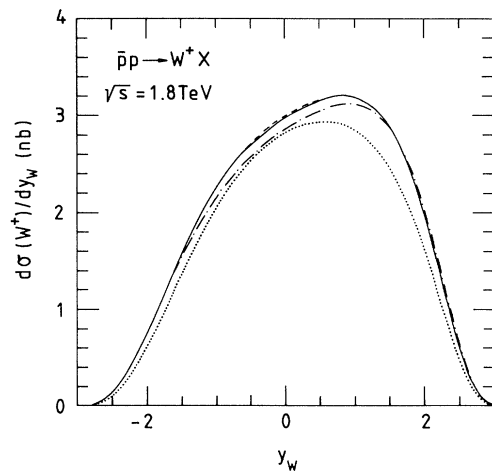


FIG. 15. Rapidity distribution of  $W^+$  bosons produced in  $p\bar{p}$  collisions at 1.8 TeV, as predicted by the  $S_0$  (dashed),  $D_0$  (continuous),  $D_-$  (dash-dot) parton distributions to  $O(\alpha_s)$ . The prediction of set  $B_0$  (dotted) of Ref. [7] is shown for comparison.

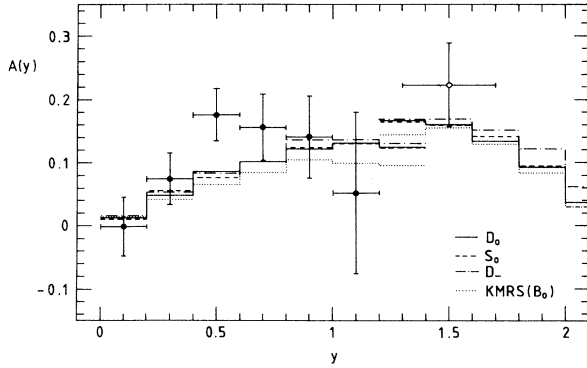


FIG. 16. Charged lepton rapidity asymmetry in  $p\bar{p}$  collisions at 1.8 TeV, as predicted by the  $S_0$  (dashed),  $D_0$  (solid),  $D_-$  (dash-dot) parton distributions, in leading-order QCD. The prediction of set  $B_0$  (dotted) of Ref. [7] is shown for comparison. The data are from the CDF Collaboration [38], with transverse mass cuts of 50 GeV (solid circles) and 60 GeV (open circle), respectively.

the sets are constrained by the same structure function data, dominantly the  $F_2^{\mu p}$  data from BCDMS and the  $n/p$  ratio from NMC. At 1800 GeV ( $M_W/\sqrt{s} \sim 0.04$ ) we begin to see the effect of the new NMC  $F_2$  data: the predictions of the new sets are now significantly above the previous  $B_0$  prediction. This increase can be directly related to the behavior of the  $B_0$  and  $D_0$  quark distributions shown in Fig. 8. Unfortunately the CDF data are not yet precise enough to discriminate between the old and new predictions. Note that our predictions are all slightly higher than the UA2 cross-section measurements. We have investigated whether the quark distributions can be adjusted to improve the agreement, but

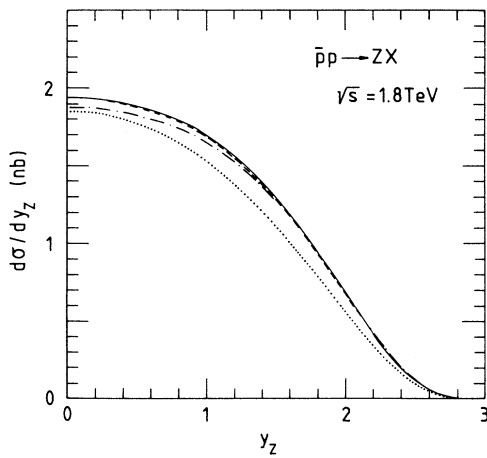


FIG. 17. Rapidity distribution of  $Z^0$  bosons produced in  $p\bar{p}$  collisions at 1.8 TeV, as predicted by the  $S_0$  (dashed),  $D_0$  (continuous),  $D_-$  (dash-dot) parton distributions, to  $O(\alpha_s)$  in QCD. The prediction of set  $B_0$  (dotted) of Ref. [7] is shown for comparison.

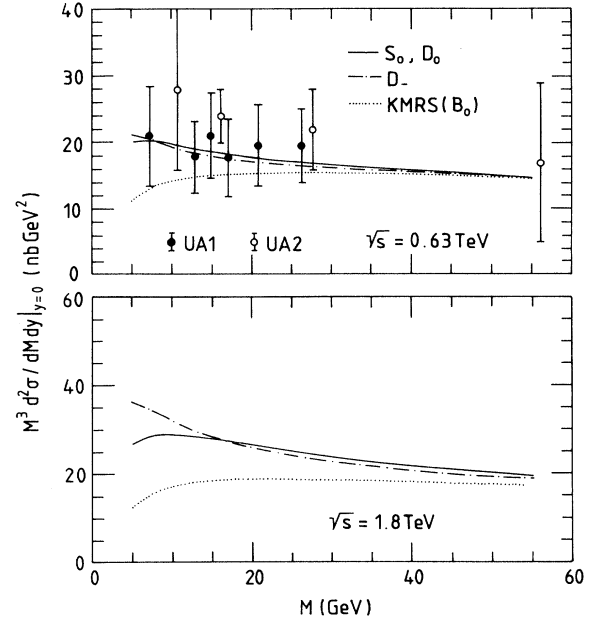


FIG. 18. The Drell-Yan cross section  $M^3 d^2\sigma/dMdy|_{y=0}$  in  $p\bar{p}$  collisions at (a) 630 GeV and (b) 1.8 TeV, as a function of the dilepton mass  $M$ . The predictions corresponding to the  $S_0$ ,  $D_0$  (continuous),  $D_-$  (dash-dot) parton distributions, calculated in  $O(\alpha_s)$  QCD, are shown. The prediction of set  $B_0$  (dotted) of Ref. [7] is shown for comparison. The data are from the UA1 and UA2 Collaborations [41]. The errors are statistical only.

we find that the deep-inelastic structure function data do not permit the  $\sim 5\%$  decrease in the quark distributions which would be required. In view of the non-negligible experimental errors and theoretical uncertainties in the calculation, we do not regard the small disagreement as significant. Note that the *ratio* of the  $W$  and  $Z$  cross sections is better described, indicating consistency with the  $n/p$  structure function ratio. The experimental measurements and the theoretical predictions at  $\sqrt{s} = 630$  GeV and 1800 GeV are summarized in Table IV. Figure 14 shows the predictions extended to higher collision energies. The main feature is the steeper increase of the cross sections for the  $D_-$  set, driven mainly by the more singular  $x^{-3/2}$  small- $x$  behavior of the sea-quark distributions. We emphasize that the spread of the predictions at energies reached at the LHC and Superconducting Super Collider (SSC) arises simply from our assumptions about the small- $x$  behavior of the parton distributions, and should not therefore be taken as indicative of the overall theoretical uncertainty. Only when HERA begins to provide information on the structure functions at small  $x$  will the predictions become more precise.

Because the  $u$ - and  $d$ -quark distributions in the proton are different,  $W^+$  ( $W^-$ ) bosons are produced preferentially in the direction of the incoming proton (antiproton) in  $p\bar{p}$  collisions. A measurement of the  $W^\pm$  rapidity *asymmetry* therefore provides information of the  $d/u$  ratio of quark distributions [31]. Figure 15 shows the  $W^+$

TABLE IV. Cross sections times leptonic branching ratios for  $W$  and  $Z$  production at  $\sqrt{s} = 630$  GeV and 1.8 TeV. The data are from the UA2 [32] and CDF [33, 37] collaborations: the first and second errors are statistical and systematic respectively. The theoretical predictions are described in the text.

	$\sqrt{s}$ (TeV)	$B\sigma_W$ (nb)	$B\sigma_Z$ (pb)	$B\sigma_W/B\sigma_Z$
$S_0$	0.63	0.768	72.8	10.55
$D_0$		0.758	73.0	10.39
$D_-$		0.750	72.8	10.31
$B_0$		0.752	71.7	10.49
Data [UA2]		$0.682 \pm 0.012 \pm 0.040$	$65.6 \pm 4.0 \pm 3.8$	$10.4 \pm_{0.6}^{0.7} \pm 0.3$
$S_0$	1.8	2.37	222	10.68
$D_0$		2.37	224	10.61
$D_-$		2.34	220	10.62
$B_0$		2.09	200	10.46
Data [CDF]		$2.19 \pm 0.04 \pm 0.21$	$209 \pm 13 \pm 17$	$10.2 \pm 0.8 \pm 0.4$

rapidity distribution at  $\sqrt{s} = 1.8$  TeV obtained from the  $S_0$ ,  $D_0$ , and  $D_-$  sets of partons, together with the previous  $B_0$  prediction for comparison. The curves are calculated in  $O(\alpha_s)$  perturbative QCD; the second-order corrections are not yet known for the rapidity distribution. Evidently, the rapidity asymmetry for all the sets is similar: the asymmetries for  $S_0$  and  $D_0$  are almost identical, and lie between those of sets  $B_0$  and  $D_-$ . What is measured in practice is of course the *charged lepton* rapidity asymmetry, defined above. In principle this carries as much information about the quark distributions as the  $W$  rapidity asymmetry, since the  $W \rightarrow l\nu$  decay is completely known. Figure 16 shows the predictions of the four sets for the lepton rapidity asymmetry, together with data from the CDF Collaboration [38]. The calculations are performed in leading order, with the same transverse mass cuts as used in the experiment. (The  $O(\alpha_s)$  correction to the asymmetry has recently been calculated [39] and shown to reduce the leading order asymmetry slightly.) Note that the highest  $y$  data point has a higher transverse mass cut, hence the discontinuity in the predictions. Overall the agreement is very satisfactory, with the new sets slightly favored. The fact that all sets give similar asymmetries can again be traced back to the fact that they are all fitted to the same  $n/p$  structure function ratio data. In Ref. [31] it was shown that the size of the asymmetry was strongly correlated with the magnitude of the *slope* of the  $n/p$  ratio in the relevant  $x$  region. In fact, the new sets have a slightly larger  $n/p$  slope than the previous  $B_0$  fit—compare Fig. 4 with Fig. 7 of Ref. [7]—and therefore the asymmetry is correspondingly slightly larger.

With the prospect of a substantial increase in integrated luminosity at the Fermilab  $p\bar{p}$  collider in the next few years, it should be possible to obtain further information on the small- $x$  quarks from the shape of the  $Z$  rapidity distribution, which can in principle be recon-

structed from the lepton four-momenta. We have already seen how the *total* cross section is indeed slightly larger at 1.8 TeV for the new sets, reflecting the larger quark distributions around  $x \sim M_Z/\sqrt{s}$ . This integrated cross section is dominated by  $Z$ 's produced with small rapidity. At larger rapidity, one of the incoming partons is forced to smaller  $x$ ,

$$x_{1,2} \sim \exp(\pm y_Z) \frac{M_Z}{\sqrt{s}}, \quad (23)$$

and we would expect the differences between the predictions based on the old and new sets to be enhanced. This is illustrated in Fig. 17, where the curves are labeled as before. (Note that the rapidity distribution is symmetric about  $y_Z = 0$ .) The effect is seen at large  $y_Z$ : the new distributions produce broader  $Z$  rapidity distributions:  $S_0$  and  $D_0$  are broader than  $B_0$ , and  $D_-$  is broader still. If there is sufficient acceptance for leptons at large rapidity, then the only issue in practice is one of statistics. Note that an integrated luminosity of  $20 \text{ pb}^{-1} \text{ yr}^{-1}$  corresponds to  $\sim 8000$  dilepton ( $e, \mu$ ) events per year at  $\sqrt{s} = 1.8$  TeV which, even allowing for efficiency losses, should be sufficient for a significant discrimination. At even higher collider energies the differences between the more singular  $D_-$ -type and the standard  $D_0$ -type distributions become apparent. For example, it was shown in Ref. [40] that at LHC and SSC energies, the singular  $D_-$ -type distributions give  $Z$  rapidity distributions which actually have maxima at large  $y_Z$ , rather than at  $y_Z = 0$ .

Figure 18 shows the Drell-Yan cross section  $M^3 d\sigma/dMdy$  at  $y = 0$  for the two collider energies, as a function of the dilepton mass  $M$ . The labeling of the curves is the same as in the previous figures. The difference between the old and new distributions is clearly seen as an enhancement of the cross sections at small mass for the latter: being proportional to the square of the parton distributions, the Drell-Yan cross section amplifies

the differences between the old and new quark distributions in the  $0.01 - 0.1-x$  range, Fig. 8. At larger dilepton masses, the predictions come together as larger  $x$  values are probed.

Also shown in Fig. 18 are recent data from the UA1 and UA2 Collaborations [41]. The errors are statistical only. The UA1 Collaboration have estimated the overall systematic error to be  $\pm 14\%$  [42]. Although it is tempting to conclude that the data favor the new distributions, it must be remembered that the predictions are calculated to  $O(\alpha_s)$  only—the second-order corrections for distributions differential in mass *and* rapidity are not yet known. Note that if we use as a guide the correction to the total (i.e., rapidity integrated) cross section [34], we might expect a rather small negative second-order correction to the differential distribution. In view of the importance of these Drell-Yan data in providing independent information on the quarks at small  $x$ , we regard the calculation of the  $O(\alpha_s^2)$  corrections to the differential distribution as a matter of some urgency. At the higher collider energy, Fig. 18(b), the differences between the old and new sets are even larger, and we also begin to see, at small dilepton masses, the appearance of the more singular small- $x$  behavior of the  $D_-$  distributions. An accurate measurement of the Drell-Yan cross section in this mass range at  $\sqrt{s} = 1.8$  TeV would be extremely useful.

#### D. Predictions for HERA

Clearly the impact of the new information that has been included in this analysis is on the physics of the small- $x$  region. Since HERA is designed to explore the region  $x/Q^2 \gtrsim 10^{-5} \text{ GeV}^{-2}$ , it is important to predict as reliably as possible the consequences of different theoretical models in order for the experimental measurements to differentiate between them. Compared to our previous analysis [7], not only are the extrapolations to  $x < 0.01$  significantly different—their reliability is much improved.

Figure 19 shows how  $F_2$  is expected to behave at low  $x$  as a result of the parton distributions shown in Fig. 8. The dramatic change in the quark distributions compared to those of  $B_0$  is reflected in expectations for  $F_2$  at  $x \approx 10^{-4}$  which are 50–80% higher than the corresponding curves in Fig. 12 of Ref. [7]. HERA probes the kinematic region in which shadowing corrections suppress the effects of the singular behavior of the gluon and sea-quark distributions of the  $D_-$ -type solution. The  $D_-(R=5)$  curve in Fig. 19 shows the effect of conventional shadowing for which we assume the partons are uniformly spread throughout the proton with radius  $R = 5 \text{ GeV}^{-1}$ . The effects of the more extreme form of shadowing, in which it is assumed that the partons are concentrated in “hot spots,” are shown by the  $D_-(R=2)$  curve. Given the precision with which HERA eventually expects to measure  $F_2$  there is a reasonable chance of distinguishing between the various assumptions for the behavior of partons. Figure 20 shows the expectations at other values of  $Q^2$  including the ranges of  $x$  and  $Q^2$  which can be probed by  $ep$  collisions at LHC.

As emphasized before, the measurement of the longitudinal structure function  $F_L$  at small  $x$ , although more

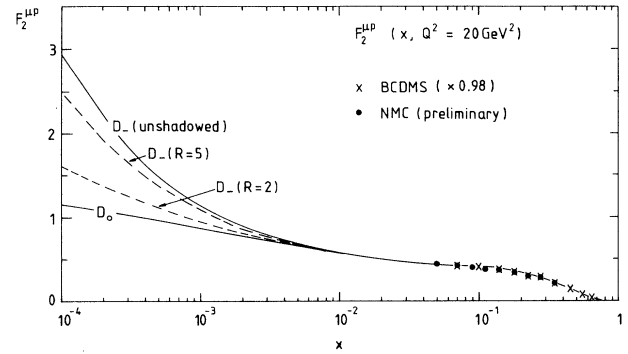


FIG. 19. The structure function  $F_2^{\mu p} (= F_2^{ep})$  shown as a function of  $x$  at  $Q^2 = 20 \text{ GeV}^2$  for the  $D_-$  and  $D_0$  set of partons (together with data used in the fits). The dashed curves show the effect of conventional ( $R = 5 \text{ GeV}^{-1}$ ) and “hot spot” ( $R = 2 \text{ GeV}^{-1}$ ) shadowing on the  $D_-$  prediction. This plot should be compared with Fig. 12 of Ref. [7] which gives the extrapolations of  $F_2^{\mu p}$  obtained from the KMRS sets of partons.

difficult than that of  $F_2$ , is much more sensitive to the nature of the gluon. Figure 21 illustrates the intimate connection between  $F_L$  and  $xg$  at small  $x$  which can be exploited to extract a much more precise estimate of the gluon distribution [43]. For completeness, we note that inelastic  $J/\psi$  production at HERA has also been advo-

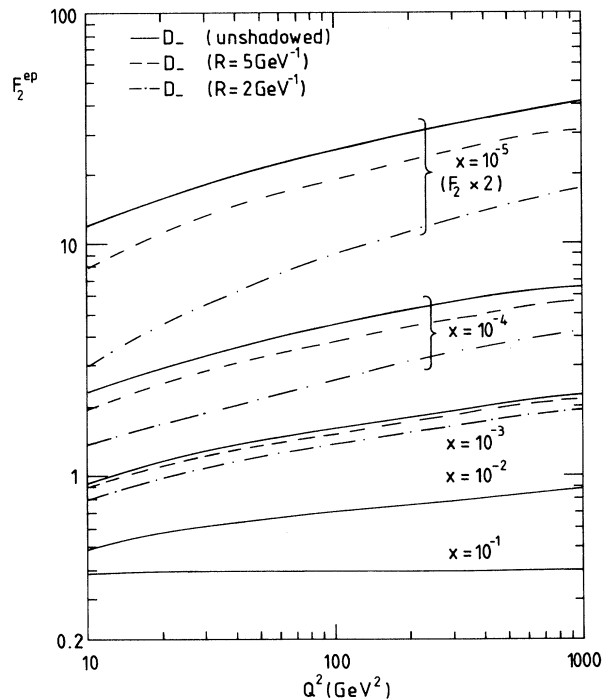


FIG. 20. Predictions for  $F_2^{ep}(x, Q^2) = F_2^{\mu p}(x, Q^2)$  shown as a function of  $Q^2$  for  $x = 10^{-1}, 10^{-2}, \dots, 10^{-5}$ . The curves correspond to the  $D_-$  fit, unshadowed and shadowed with  $R = 5$  and  $2 \text{ GeV}^{-1}$ .

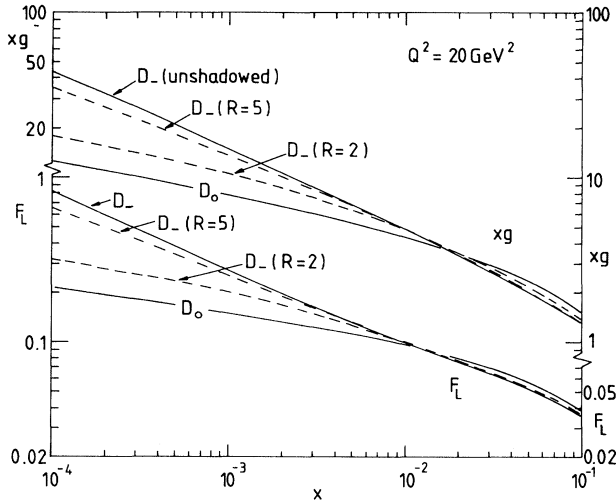


FIG. 21. The upper and lower sets of curves correspond, respectively, to the gluon distribution  $xg(x, Q^2)$  and the longitudinal structure function  $F_L(x, Q^2)$  as functions of  $x$  at  $Q^2 = 20 \text{ GeV}^2$ . The continuous curves correspond to the  $D_-$  and  $D_0$  predictions and the dashed curves show the effects of shadowing on the  $D_-$  curve.

cated [44] as a promising measurement of the small- $x$  behavior of the gluon. A recent comprehensive review of  $J/\psi$  production has been given by Jung *et al.* [45].

Perturbative QCD predicts [46] a singular  $x^{-\lambda}$  behavior of the gluon and sea-quark distributions, as typified by our  $D_-$  set of partons. Indeed this small- $x$  behavior is characteristic of the leading  $\log(1/x)$  summation of multiple soft gluon emissions. However, as we have seen, no experimental data yet exist to distinguish this so-called ‘‘Lipatov’’ behavior from the more traditional small- $x$  behavior of the  $D_0$  and  $S_0$  sets. Although measurements of  $F_2$ ,  $F_L$ , and  $J/\psi$  at HERA should be able to probe the relevant small- $x$  region, it has been advocated [47] that the ‘‘Lipatov’’  $x^{-\lambda}$  behavior can be more cleanly identified by observing small- $x$  deep-inelastic events which contain a measured jet. The application of this method [48] at HERA will rely on the parton distributions being reliably known for  $x \gtrsim 0.01$ , but not at smaller  $x$ .

## V. CONCLUSIONS

There are several reasons why it is important to have parton distributions which are as accurate as possible. First, the very fact that it is possible to extract a *consistent* set from the growing amount of high-precision data covering a wide number of different processes is itself an impressive acknowledgment of the validity of the underlying theory. Second, the improvement in precision of the parton distributions allows increasingly reliable estimates to be made for processes in new kinematic ranges, in particular at higher energies. The ‘‘Martin-Roberts-Stirling (MRS) philosophy’’ is to continually update and improve the parton distributions as new experimental information becomes available. This program is complementary

to the advances in the calculation of even higher order perturbative QCD corrections.

Recent deep-inelastic scattering data from NMC [4] have shed new light on the region  $0.01 < x < 0.1$ , as well as confirming existing measurements at larger  $x$ . These new data lead to an increase in previous estimates of the parton distributions (based largely on extrapolation) below  $x \sim 0.05$ , and also appear to confirm the previous result that the value of the Gottfried sum rule is most likely less than the contribution from valence quarks alone. The natural way to accommodate this result is to relax the  $\bar{u} = \bar{d}$  constraint assumed in all previous parton distribution analyses. In the present study we provide parton distributions with or without the  $\bar{u} = \bar{d}$  constraint (S or D type) and show that the D type is indeed a more natural choice. It would be interesting to find an independent phenomenological preference for either S or D solutions. This seems to be hard, for example, the  $\bar{p}p \rightarrow W, Z$  cross sections, being largely dominated by valence-valence collisions, are quite insensitive to the choice. The most promising route, which we will address in a future study, appears to be in comparing Drell-Yan production in  $pp$  and  $pn$  collisions [49].

There are new data also on neutrino deep-inelastic scattering from the CCFR Collaboration which we have included. Consistency with other deep-inelastic data is achieved if the CCFR data are shifted down by 6%, but more significantly these new data show a vastly improved agreement with the  $Q^2$  behavior expected from perturbative QCD.

We stress the importance of examining *all* processes that involve the parton distributions. We have considered several cases where there are direct connections between features of deep-inelastic scattering and of hadronic reactions. For example, the *ratio* of the  $W$  and  $Z$  cross sections in  $\bar{p}p$  collisions is tied to the *ratio*  $n/p$  of the structure functions at  $x \sim M_V/\sqrt{s}$ , while the *asymmetry* of the  $W^\pm$  rapidity distributions is governed by the *slope* of the  $n/p$  ratio at that  $x$  value. The *magnitude* of the  $W$  cross section is rigidly constrained by the *size* of  $F_2$  at  $x \sim M_W/\sqrt{s}$  and so the cross sections at the CERN Super Proton Synchrotron (SPS) collider are already tightly constrained by the previous structure function measurements at  $x \sim 0.13$ , while those at the Fermilab collider are influenced by the new NMC measurement of  $F_2$  around  $x \sim 0.04$ . Likewise, in the future predictions at LHC and/or SSC will be based on structure function measurements at HERA in the region  $x \sim 0.005$ .

Of course we can already make predictions for the very small- $x$  region based on extrapolations of our fits, but the major uncertainty arises from the assumed behavior of the gluon and sea-quark distributions. As a measure of this uncertainty we provide two possible sets of partons, one ( $D_0$ ) based on ‘‘finite’’ gluons and sea quarks as  $x \rightarrow 0$  and the other ( $D_-$ ) based on singular forms  $\sim x^{-\lambda}$  which have theoretical justification based on resumming soft gluon emissions. However this ‘‘Lipatov’’ gluon is almost certainly softened by some shadowing correction the size of which, in turn, is a matter of debate. We have therefore provided another two parton sets which choose either a conventional shadowing correction (with radius

$R = 5 \text{ GeV}^{-1}$ ) or one corresponding to the “hot spot” scenario (with radius  $R = 2 \text{ GeV}^{-1}$ ). One of the aims of this analysis is to suggest phenomenological “pointers” which will hopefully reveal the gluon’s nature. We have studied the consequences of the different solutions for measurements of  $F_2$  and  $F_L$  at HERA, and the indications are that the latter, together with the measurement of  $J/\psi$  production, will reveal the correct small- $x$  behavior. But in the long term it will be the high-energy proton-proton colliders which will provide quantitative tests of the really small- $x$  behavior—again,  $W$  and  $Z$  production will be an important tool.

Finally, while we have concentrated on the impact of new experimental information on the small- $x$  region, we should emphasize that there has been little change in the

situation at  $x > 0.1$  (see Fig. 8). Our previous analyses [50] of processes such as top-quark and large  $p_T$  jet production in high-energy  $p\bar{p}$  collisions, which are not sensitive to the small- $x$  region, are still valid.

#### ACKNOWLEDGMENTS

We are grateful to Michiel Botje, Henry Frisch, Eva-Maria Kabuss, Steve Kuhlmann, Ger Van Middelkoop, Alexander Moulin, and Hatti Plathow-Besch for useful discussions and communications concerning the experimental data. We would also like to thank Willy Van Neerven and Ellen Zijlstra for supplying the program for the second-order calculation of the  $W$  and  $Z$  cross sections.

- 
- [1] P.N. Harriman, A.D. Martin, R.G. Roberts, and W.J. Stirling, *Phys. Rev. D* **42**, 798 (1990); J. Kwiecinski, A.D. Martin, R.G. Roberts, and W.J. Stirling, *ibid.* **42**, 3645 (1990); J. Morfin and W.K. Tung, *Z. Phys. C* **52**, 13 (1991); M. Diemoz, F. Ferroni, E. Longo, and G. Martinelli, *Z. Phys. C* **39**, 21 (1988).
- [2] See, for example, H. Plathow-Besch, in *Proceedings of the Third Workshop on Detector and Event Simulation in High Energy Physics*, Amsterdam, 1991.
- [3] Recent reviews are A.D. Martin, *Acta Phys. Pol.* **B22**, 1095 (1991); B. Badelek, K. Charchula, M. Krawczyk, and J. Kwiecinski, *Rev. Mod. Phys.* **64**, 927 (1992); E. M. Levin, Report No. DESY 91-110.
- [4] NMC, M.W. van der Heijden, thesis, University of Amsterdam, 1991; E. Kabuss, invited talk at DESY-Zeuthen Workshop on Deep Inelastic Scattering, 1992; see also [14].
- [5] CCFR Collaboration, S.R. Mishra, in *Proceedings of the Joint International Lepton-Photon Symposium and Europhysics Conference on High Energy Physics*, Geneva, Switzerland, 1991, edited by S. Hegarty, K. Potter, and E. Quercigh (World Scientific, Singapore, 1992), p. 135; S.R. Mishra, presented at the 26th Conference on High Energy Physics, Dallas, Texas, 1992 (unpublished).
- [6] CDHSW Collaboration, J.P. Berge *et al.*, *Z. Phys. C* **49**, 187 (1990).
- [7] J. Kwiecinski, A.D. Martin, R.G. Roberts, and W.J. Stirling, *Phys. Rev. D* **42**, 3645 (1990) (abbreviated KMRS).
- [8] NMC, P. Amaudruz *et al.*, *Phys. Rev. Lett.* **66**, 2712 (1991).
- [9] K. Gottfried, *Phys. Rev. Lett.* **18**, 1174 (1967).
- [10] A.D. Martin, R.G. Roberts, and W.J. Stirling, *Phys. Lett. B* **252**, 653 (1990).
- [11] EMC, J.J. Aubert *et al.*, *Nucl. Phys.* **B259**, 189 (1985); K.A. Bazizi, thesis, University of California Riverside, 1991.
- [12] BCDMS Collaboration, A.C. Benvenuti *et al.*, *Phys. Lett. B* **223**, 485 (1989).
- [13] K. Bazizi, S.J. Wimpenny, and T. Sloan, in *Proceedings of the 25th International Conference on High Energy Physics*, Singapore, 1990, edited by K.K. Phua and Y. Yamaguchi (World Scientific, Singapore, 1991).
- [14] The final NMC data have recently (27th July 1992) become available [15]. These data are essentially identical to the preliminary version of the NMC data [4] that we have used, and do not change our results. The only significant changes between the preliminary and the final NMC data occur at their lower beam energy and at low  $Q^2$ , that is, in data which fall outside the cuts that have been applied in our analysis.
- [15] NMC, P. Amaudruz *et al.*, CERN Report No. PPE/92-124 (1992).
- [16] WA70 Collaboration, M. Bonesini *et al.*, *Z. Phys. C* **38**, 371 (1988).
- [17] A.D. Martin, W.J. Stirling, and R.G. Roberts, *Phys. Lett. B* **228**, 149 (1989).
- [18] CCFR Collaboration, C. Foudas *et al.*, *Phys. Rev. Lett.* **64**, 1207 (1990).
- [19] NMC, P. Amaudruz *et al.*, *Nucl. Phys.* **B371**, 3 (1992).
- [20] BCDMS, A.C. Benvenuti *et al.*, *Phys. Lett. B* **237**, 599 (1990).
- [21] EMC, J.J. Aubert *et al.*, *Nucl. Phys.* **B293**, 740 (1987).
- [22] E605 Collaboration, C.N. Brown *et al.*, *Phys. Rev. Lett.* **63**, 2637 (1989).
- [23] R.G. Roberts and M.R. Whalley, *J. Phys. G* **17**, D1 (1991).
- [24] L.W. Whitlow, E.M. Riordan, S. Dasu, S. Rock, and A. Bodek, *Phys. Lett. B* **282**, 475 (1992).
- [25] A.D. Martin, W.J. Stirling, and R.G. Roberts, *Phys. Lett. B* **266**, 173 (1991).
- [26] M. Virchaux and A. Milsztajn, *Phys. Lett. B* **272**, 221 (1992).
- [27] T. Hebbeker, in *Proceedings of the Joint International Lepton-Photon Symposium and Europhysics Conference on High Energy Physics* [5], p. 73.
- [28] P. Aurenche and M.R. Whalley, Durham-RAL HEP Database, RAL Report No. 89-106 (1989).
- [29] L.N. Epele, H. Fanchiotti, C.A. Garcia Canal, and R. Sassot, *Phys. Lett. B* **275**, 155 (1992).
- [30] B. Badelek and J. Kwiecinski, *Nucl. Phys.* **B370**, 278 (1992).
- [31] A.D. Martin, R.G. Roberts, and W.J. Stirling, *Mod. Phys. Lett. A* **4**, 1135 (1989).
- [32] UA2 Collaboration, J. Alitti *et al.*, *Phys. Lett. B* **276**, 365 (1992).
- [33] CDF Collaboration, F. Abe *et al.*, *Phys. Rev. D* **44**, 29 (1991).
- [34] R. Hamberg, W.L. Van Neerven, and T. Matsuura, *Nucl.*

- Phys. **B359**, 343 (1991).
- [35] UA2 Collaboration, J. Alitti *et al.*, Phys. Lett. B **276**, 354 (1992); CDF Collaboration, F. Abe *et al.*, Phys. Rev. D **43**, 2070 (1991).
- [36] J. Carter, in *Proceedings of Joint International Lepton-Photon Symposium and Europhysics Conference on High Energy Physics* [5] p. 1.
- [37] CDF Collaboration, F. Abe *et al.*, Phys. Rev. Lett. **64**, 152 (1990).
- [38] CDF Collaboration, F. Abe *et al.*, Phys. Rev. Lett. **68**, 1458 (1992).
- [39] H. Baer and M.H. Reno, Phys. Rev. D **43**, 2892 (1991).
- [40] A.D. Martin and W.J. Stirling, Phys. Lett. B **248**, 443 (1990).
- [41] UA1 Collaboration, A. Moulin, in *Proceedings of the 21st International Symposium on Multiparticle Dynamics*, Wuhan, China, 1991, edited by L. Liu and Y. Wu (World Scientific, Singapore, 1992); UA2 Collaboration, J. Alitti *et al.*, Phys. Lett. B **275**, 202 (1992).
- [42] A. Moulin (private communication).
- [43] A.M. Cooper-Sarkar, G. Ingelman, K.R. Long, R.G. Roberts, and D.H. Saxon, Z. Phys. C **39**, 281 (1988).
- [44] E.L. Berger and D. Jones, Phys. Rev. D **23**, 1521 (1981); A.D. Martin, C.-K. Ng, and W.J. Stirling, Phys. Lett. B **191**, 200 (1987); NM Collaboration, D. Allasia *et al.*, Phys. Lett. B **258**, 493 (1991).
- [45] H. Jung, G.A. Schuler, and J. Terron, in *Proceedings of the Workshop on Physics at HERA*, Hamburg, Germany, 1991, edited by W. Buchmuller and G. Ingelman (DESY, Hamburg, in press) Vol. 2, p. 721.
- [46] E.A. Kuraev, L.N. Lipatov, and V.S. Fadin, Zh. Eksp. Teor. Fiz. **72**, 377 (1977) [Sov. Phys. JETP **45**, 199 (1977)]; Ya. Balitsky and L.N. Lipatov, Yad. Fiz. **28**, 1597 (1978) [Sov. J. Nucl. Phys. **28**, 822 (1978)].
- [47] A.H. Mueller, in *Proceedings of the Topical Workshop on the Small- $x$  Behavior of Deep Inelastic Scattering Structure Functions in QCD*, Hamburg, Germany, 1990, edited by A. Ali and J. Bartels [Nucl. Phys. B (Proc. Suppl.) **18C**, 125 (1990)]; J. Phys. G **17**, 1443 (1991).
- [48] J. Bartels, A. De Roeck, and M. Loewe, Z. Phys. C **54**, 635 (1992); W.-K. Tang, Phys. Lett. B **278**, 363 (1992); J. Kwiecinski, A.D. Martin, and P.J. Sutton, Phys. Rev. D **46**, 921 (1992); Phys. Lett. B **287**, 254 (1992).
- [49] S.D. Ellis and W.J. Stirling, Phys. Lett. B **256**, 258 (1991).
- [50] A.D. Martin, W.J. Stirling, and R.G. Roberts, Phys. Rev. D **43**, 3648 (1991).